arXiv:1611.03198v1 [cond-mat.quant-gas] 10 Nov 2016

Exploring Few-Body Processes with an Ultracold Light-Heavy Bose-Bose Mixture

Fudong Wang,[1,*] Xin Ye,[1] Mingyang Guo,[1] D. Blume,[2] and Dajun Wang[1,3,†]

[1] *Department of Physics, The Chinese University of Hong Kong, Hong Kong, China*
[2] *Department of Physics and Astronomy, Washington State University, Pullman, WA 99164-2814, USA*
[3] *The Chinese University of Hong Kong Shenzhen Research Institute, Shenzhen, China*

(Dated: November 11, 2016)

We report the observation of several few-body processes with an ultracold Bose-Bose mixture consisting of sodium and rubidium atoms and weakly-bound NaRb Feshbach dimers. Preparing a pure dimer sample and tuning the scattering length between Na and Rb via a magnetic Feshbach resonance, a resonant loss feature tied to a Na_2Rb_2 tetramer state is observed. Preparing an atom-dimer mixture, a resonance associated with a $NaRb_2$ trimer is also observed. A theoretical framework that reproduces the experimental observations of the resonance positions qualitatively is developed. Our combined experiment-theory study provides a first step toward understanding universal low-energy three- and four-body processes in heteronuclear Bose-Bose mixtures, has practical implications for molecule production in heteronuclear mixtures, and underlines that much remains to be explored before a fully satisfactory picture of few-body processes in heteronuclear Bose-Bose mixtures can be painted.

I. INTRODUCTION

A. Few-body Efimov physics

One of the most amazing features of few-body physics is the existence of universality across systems governed by vastly different energy scales. Efimov resonances, which were originally predicted for nuclear systems [1] but were first verified with ultracold atoms [2], are a prominent example. In the Efimov scenario [1, 3], three-body bound states known as Efimov trimers emerge when the magnitude of at least two of the pairwise interactions in a three-particle system are tuned to large values, i.e., when the two-body s-wave scattering length a is much larger than the range of the interaction potential. The binding energies of successive Efimov trimers are related discretely by a simple universal scaling factor $\lambda^2 = e^{2\pi/s_0}$ [1, 3], where s_0 is determined by the statistics of the particles, their mass ratios, and the number of resonant pairwise interactions [3–6]. Intriguingly, Efimov trimers exist not only for $a > 0$, where two-body bound states are supported, but also for $a < 0$, where no weakly-bound two-body bound states exist. When $|a|$ is smaller than the range of the interaction potential, Efimov states are absent entirely.

Ultracold atom systems have become the primary platform for testing Efimov physics due to the capability of controlling scattering lengths via magnetic Feshbach resonances [7]. Indeed, since the first experimental cold-atom observation in 2006 [2], Efimov physics has been studied extensively in several homonuclear [8–12] and heteronuclear systems [13–18]. The strongly mass-imbalanced Li-Cs mixture, e.g., featuring a larger s_0 value than the three identical boson system, results in a notably reduced scaling factor. The reduced scaling factor facilitated the observation of three Efimov resonances on the $a < 0$ side [15, 16] (here, a denotes the interspecies s-wave scattering length), which in turn triggered extensive efforts to understand the Efimov scaling in the presence of a non-resonant, non-vanishing intraspecies s-wave scattering length [19, 20]. Moreover, a tiny hump in the loss spectrum was interpreted [20] as being consistent with a theoretical prediction for where the four-body $LiCs_3$ state hits the four-atom continuum [21]. The $a > 0$ side, in contrast, has been investigated comparatively little for heteronuclear systems. While an atom-dimer resonance was observed in the ^{40}K-^{87}Rb system [14], no experimental results have been reported yet for the heteronuclear four-body sector, despite the fact that some theoretical predictions exist [21–23].

A very convenient candidate for investigating four-body physics is an ultracold gas of weakly-bound Feshbach molecules (FMs). In the homonuclear Cs_2 dimer gas, Feshbach-like resonances were observed around an atomic g-wave Feshbach resonance [24] and a loss minimum, rather than a resonance, was reported in the halo-dimer regime [25]. Later on, D'Incao *et al.* [26] interpreted this loss minimum as the region between two dimer-dimer Feshbach-like resonances ($a^*_{\mathrm{dd},i}$ with $i = 1$ and 2 in Ref. [26]) that are associated with four-body states. The positions of these resonances are given by two universal relations that connect $a^*_{\mathrm{dd},i}$ with the scattering length a^*_{ad} at which the atom-dimer resonance occurs. For identical bosons, it has been theoretically predicted [27, 28] and experimentally verified [29] that there exist exactly two such four-body states tied to each Efimov trimer. For a mixture consisting of light bosons (L) and heavy bosons (H), the situation is significantly more complicated since there may exist two distinct heteronuclear trimers (LH_2 and L_2H) and three distinct tetramers (L_3H, L_2H_2 and LH_3) [21–23].

In this work, we experimentally and theoretically investigate several heteronuclear three- and four-body pro-

* Current address: Department of Physics, University of Toronto, M5S 1A7 Canada
† djwang@phy.cuhk.edu.hk

cesses with the ultracold ^{23}Na-^{87}Rb system [30, 31], which is characterized by the mass ratio $\kappa = m_{\rm Rb}/m_{\rm Na} \approx 3.78$ with $m_{\rm Rb}$ and $m_{\rm Na}$ denoting the atomic mass of ^{87}Rb and ^{23}Na, respectively. Our experimental studies focused on the interspecies scattering length $a > 0$ side where NaRb FMs can be created by magneto-association [32]. In a sample of pure FMs, we observed a dimer-dimer loss resonance, which is attributed to a Na_2Rb_2 tetramer state. An atom-dimer resonance that is related to the $NaRb_2$ Efimov trimer was measured in a mixture of NaRb FMs and Rb atoms. Theoretical calculations based on the adiabatic hyperspherical framework for zero-range interactions yielded an Rb-NaRb atom-dimer resonance position in good agreement with the experimentally measured one and predicted the position of a Na-NaRb atom-dimer resonance, without input besides the two-body scattering lengths. Using this information, a low-energy description of the four-body systems Na_2Rb_2 and $NaRb_3$ was developed. The qualitative agreement between experiment and theory allowed us to propose a generalized Efimov scenario for heavy-light Bose-Bose mixtures.

B. Overview of light-heavy Bose-Bose mixture

The goal of the present work is to obtain a first understanding of the universal three- and four-body processes, or absence thereof, in ultracold light-heavy Bose-Bose mixtures with large positive interspecies scattering length. In the ideal Efimov scenario, where the Rb-Rb and Na-Na scattering lengths vanish, the scaling factors for the $NaRb_2$ and Na_2Rb systems are $\lambda_{\rm NaRbRb} = 37$ and $\lambda_{\rm NaNaRb} = 5.1 \times 10^8$, respectively. These large scaling factors make it experimentally demanding if not impossible to observe features associated with consecutive three-body Efimov states. However, the relationship between the critical scattering lengths associated with a $NaRb_2$ Efimov trimer and a Na_2Rb Efimov trimer (denoted by $a^*_{\rm ad,Rb}$ and $a^*_{\rm ad,Na}$, respectively, in Fig. 1) or that associated with a $NaRb_2$ Efimov trimer and one of the four-body states (the scattering length for one such state is denoted by $a^*_{\rm dd}$ in Fig. 1) provides an alternative route to experimentally deduce information about the generalized light-heavy Bose-Bose Efimov scenario.

Since four-body processes in light-heavy Bose-Bose mixtures have never been explored experimentally and since the theoretical description of the four-body sectors is still in its infancy, we start our discussion by introducing the relevant system parameters. The two-body system parameters are the mass ratio κ, the light-light, heavy-heavy and light-heavy scattering lengths (denoted by $a_{\rm LL}$, $a_{\rm HH}$ and a), and the light-light, heavy-heavy and light-heavy van der Waals lengths. Either the scattering lengths at which the trimers hit the three-atom threshold or the binding energies at unitarity can be used to define the three-body parameters. For homonuclear systems, it was found that the three-body parameter is, with about

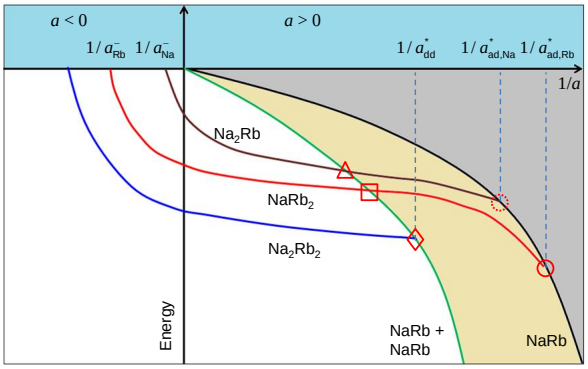

FIG. 1. Schematic few-body energy spectrum of the Na-Rb system. The binding energies for one and two NaRb dimers, the $NaRb_2$ and Na_2Rb trimers and the Na_2Rb_2 tetramer are shown as a function of $1/a$. To enhance the readability, several other trimers and tetramers are not shown. The shaded area above zero energy is the atomic scattering continuum, while the yellow and gray shaded areas represent the dimer-dimer and atom-dimer scattering continuum, respectively. The observed resonances for NaRb + NaRb at $a^*_{\rm dd}$ and Rb + NaRb at $a^*_{\rm ad,Rb}$ are marked by the diamond and the solid red circle, respectively. The, as of yet, experimentally unconfirmed Na + NaRb resonance at $a^*_{\rm ad,Na}$ is marked by the dotted red circle. The red square and triangle indicate the thresholds of the rearrangement reactions NaRb + NaRb $\rightarrow$ $NaRb_2$ + Na and NaRb + NaRb $\rightarrow$ Na_2Rb + Rb, respectively. The corresponding scattering lengths (not marked) are $a^{\rm reaction}_{\rm dd,Rb}$ and $a^{\rm reaction}_{\rm dd,Na}$. On the $a < 0$ side, the "Efimov favored" $NaRb_2$ and the "Efimov unfavored" Na_2Rb trimers intersect the three-atom continuum at $a^-_{\rm Rb}$ and $a^-_{\rm Na}$, respectively.

15% accuracy, determined by the van der Waals length, i.e., the three-body parameter was found to be determined, to a good approximation, by two-body parameters [33–35]. Reference [36, 37] suggested that this notion could be extended to heteronuclear three-body van der Waals systems, in which the identical particles are either bosons or fermions; unfortunately, however, the emergent universality appeared to be rather complicated.

Very recently [20], it was suggested that a zero-range theory that is based on the inter- and intraspecies two-body scattering lengths alone predicts a subset of the $^{133}Cs_2{}^6Li$ (^{133}Cs is a composite boson) properties on the negative interspecies scattering length side qualitatively. Application of this model to the positive interspecies scattering length side (see Sec. III A) predicts that the atom-dimer scattering length $a^*_{\rm ad,Na}$ at which the lowest Na_2Rb Efimov trimer in the "upper" Efimov branch (there exists a "lower" and an "upper" Efimov branch [20]) merges with the Na-NaRb atom-dimer threshold is larger than the atom-dimer scattering length $a^*_{\rm ad,Rb}$ at which the lowest $NaRb_2$ Efimov trimer in the upper Efimov branch merges with the Rb-NaRb atom-dimer threshold. The open circles in Fig. 1 mark the scattering lengths at which enhanced losses due to the energetic degeneracy of the trimers and the NaRb dimer should be observable experimentally. Indeed, Sec. II B

reports the experimental observation of one of these resonances.

In the four-body sector, resonant loss features associated with processes that involve Na_2Rb_2, Na_3Rb, and $NaRb_3$ should, in principle, be observable. The latter two tetramers, Na_3Rb and $NaRb_3$, are expected to be tied to the Na_2Rb and $NaRb_2$ trimers, respectively. At unitarity, the existence of one LH_3 tetramer tied to each LH_2 trimer was predicted for the mass ratio 8 [21]. This tetramer is expected to exist on the positive interspecies scattering length side till the tetramer energy hits the LH+H+H or LH_2+H thresholds. Whether such a tetramer state exists for the smaller Rb-Na mass ratio of 3.78 is presently unknown. Moreover, near the dimer+atom+atom threshold, a new sequence of effective three-body Efimov states consisting of a tightly-bound light-heavy dimer and two atoms has been predicted to exist for mass ratios 30 and 50 [23]. Whether such effective three-body Efimov states exist for much smaller mass ratios is presently unknown. Last, whether Na_3Rb tetramers—attached to the so-called Efimov unfavored Na_2Rb trimer—exist, has, to the best of our knowledge, not yet been studied.

This work focuses on Na_2Rb_2 tetramers, which can be probed experimentally via collisions between two NaRb dimers in an ultracold molecular NaRb sample. Theoretically, this four-body system is particularly interesting as it contains the $NaRb_2$ and Na_2Rb trimer subsystems. Thus, it is *a priori* not clear, if the Na_2Rb_2 tetramer is, at least predominantly, associated with one of the two sub-Efimov trimers. Our finite-range low-energy Hamiltonian, which is constructed to roughly reproduce the energies of the Na_2Rb and $NaRb_2$ trimers obtained within the zero-range framework (see Sec. III B for details), predicts the existence of one Na_2Rb_2 tetramer that lies below the $NaRb_2$ trimer and, roughly, traces the energy of this trimer (see Fig. 1 for a schematic). The critical scattering length $a^*_{\rm dd}$ is found to be, theoretically and experimentally, larger than the critical scattering length $a^*_{\rm ad,Rb}$. The next section discusses our experimental studies and Sec. III presents the theoretical models. The interpretation of the data is presented in Sec. IV. Lastly, Sec. V presents an outlook.

II. EXPERIMENT

A. Feshbach resonance and Feshbach molecules

The starting point of our experiment is an ultracold mixture of Rb and Na atoms both in their lowest hyperfine Zeeman level $|F=1, m_F=1\rangle$, where F is the atomic hyperfine quantum number and m_F the corresponding projection quantum number. The interspecies s-wave scattering length a is tuned using the Feshbach resonance located at $B_0 = 347.64$ G [30, 32]. In the vicinity of B_0, the dependence of a on the magnetic field strength B is given by

$$a = a_{\rm bg}\left(1-\frac{\Delta}{B-B_0}\right)\left(1-\frac{\Delta_1}{B-B_1}\right), \qquad (1)$$

with the background scattering length $a_{\rm bg} = 66.8a_0$ (a_0 is the Bohr radius) and the resonance width $\Delta = 5.20$ G as measured by radio frequency association spectroscopy [32]. The second term in round brackets on the right hand side of Eq. (1) accounts for the influence of a nearby resonance located at $B_1 = 478.83$ G with width $\Delta_1 = 4.81$ G.

For the magnetic field strengths considered, the Rb-Rb and Na-Na scattering lengths are approximately constant, $a_{\rm RbRb} = 100.4a_0$ [38] and $a_{\rm NaNa} = 54.5a_0$ [39]. The fact that these scattering lengths are finite and positive has, as we will show in this work, an appreciable effect on the critical scattering length values at which the Efimov trimers hit the atom-dimer threshold. For positive and large interspecies scattering length a, weakly-bound Feshbach NaRb molecules can be obtained. Universal or semi-universal physics is expected to emerge if a, in absolute value, is sufficiently large.

The precise determination of a is essential for the analysis and for connecting experiment and theory. Presently, the B-to-a-conversion is limited by two factors. First, the parameters entering into Eq. (1) have uncertainties [30]. Second, because of the relatively small $a_{\rm bg}$ and Δ, the magnetic field needs to be tuned rather close to B_0 to obtain large a. This implies that the short-term magnetic field stability of about ± 7 mG translates into a non-negligible uncertainty of a for magnetic field strengths near B_0. For the smallest $|B-B_0|$ considered in this work, i.e., for $B = 347.480(7)$ G, Eq. (1) yields $a = 2320(98)a_0$. A new magnetic field system with better stability and faster response times, which will allow for an improved characterization of the Feshbach resonance, is currently under development.

To create FMs, we start with an atomic mixture at $B = 355$ G ($a = 20.3a_0$) and then sweep across the resonance to $B = 335.62$ G ($a = 98.9a_0$) to do the magneto-association. The interspecies scattering length a and the binding energy of the FMs can then be controlled by changing the magnetic field strength between 335.62 G and 347.48 G, corresponding to binding energies ranging from about $2\pi \times 22$ MHz to $2\pi \times 19$ kHz [30], which are comparable to or smaller than the van der Waals energy of $2\pi \times 17.6$ MHz. Last, for detection, the magnetic field is swept reversely across the resonance to dissociate the FMs. The resulting atoms are imaged using standard absorption imaging methods.

B. Atom-dimer collisions

To investigate the collisions between Rb and NaRb, we selectively remove residual Na atoms after the magneto-association. To this end, we first transfer the Na atoms to the $|2,2\rangle$ hyperfine Zeeman level with a microwave

rapid adiabatic passage and then drive the cycling transition with a resonant light pulse. Afterward, the magnetic field strength is increased to the desired value and the time evolution of both the atoms and the molecules is measured. The remaining molecules are detected by looking at the Na signal.

In principle, both atom-molecule and molecule-molecule collisions can cause the loss of molecules in an atom-molecule mixture. However, since the number of atoms in our experiments is typically 10 times larger than the number of molecules, the molecule loss induced by atom-molecule collisions is much faster than that induced by inelastic molecule-molecule collisions. Figure 2(a) exemplarily shows the time evolution of the NaRb molecule number at $B = 344.31$ G. It can be seen that the molecule loss happens on a time scale of less than 10 ms. On this time scale, molecule-molecule collisional loss is, as will be shown in Sec. II C, negligible. Moreover, the Rb atom number time evolution data shown in Fig. 2(b), which are taken together with the data shown in Fig. 2(a), demonstrate that the loss of atoms is also negligible on the same time scale. In what follows we thus assume that the data in Fig. 2(a) are governed by the Rb-NaRb loss rate coefficient $\beta_{\mathrm{ad,Rb}}$.

The temperature of the Rb cloud is measured to be $T_{\mathrm{Rb}} = 255(20)$ nK with time-of-flight expansion. Since we observe no changes of T_{Rb} on the time scale of the measurement, the average number density $\langle n_{\mathrm{Rb}} \rangle = [m_{\mathrm{Rb}} \bar{\omega}_{\mathrm{Rb}}^2/(2\pi k_B T_{\mathrm{Rb}})]^{3/2} N_{\mathrm{Rb}}/\sqrt{8}$ of the Rb atoms should be constant. Here a Gaussian distribution for thermal samples in a harmonic trap is assumed with $\bar{\omega}_{\mathrm{Rb}}$, N_{Rb} and k_B denoting the average trap frequency ($\bar{\omega}_{\mathrm{Rb}}$ is measured to be $2\pi \times 72(1)$ Hz), the Rb atom number, and the Boltzmann constant, respectively. The rate equation

$$dN/dt = -\beta_{\mathrm{ad,Rb}} \alpha \langle n_{\mathrm{Rb}} \rangle N \tag{2}$$

for the number of molecules N then leads to an exponential time evolution:

$$N(t) = N_0 e^{-\beta_{\mathrm{ad,Rb}} \alpha \langle n_{\mathrm{Rb}} \rangle t}. \tag{3}$$

Here $\beta_{\mathrm{ad,Rb}}$ is the Rb-NaRb loss rate coefficient, N_0 is the initial molecule number and $\alpha \langle n_{\mathrm{Rb}} \rangle$ is the effective atom density experienced by the molecules, with $\alpha = 0.79$ determined by the density distributions and the differential gravity sag of the two clouds [40].

To extract $\beta_{\mathrm{ad,Rb}}$, the NaRb molecule time evolution is fit to Eq. (3). The solid line in Fig. 2(a) shows an example of such a fit for a fixed magnetic field strength B. The dependence of $\beta_{\mathrm{ad,Rb}}$ on B is summarized in Fig. 2(c), with the error bars representing the uncertainty of the fit. The systematic error of $\beta_{\mathrm{ad,Rb}}$ due to the uncertainties of the effective in-trap density $\alpha \langle n_{\mathrm{Rb}} \rangle$ amounts to $\pm 20\%$. An additional systematic uncertainty comes from the possible non-equilibrium density distribution due to the short experimental time scale, which does likely leave the samples not enough time to thermalize; we do not currently have a reliable way to estimate the systematic uncertainty due to these non-equilibrium effects. Figure 2(c)

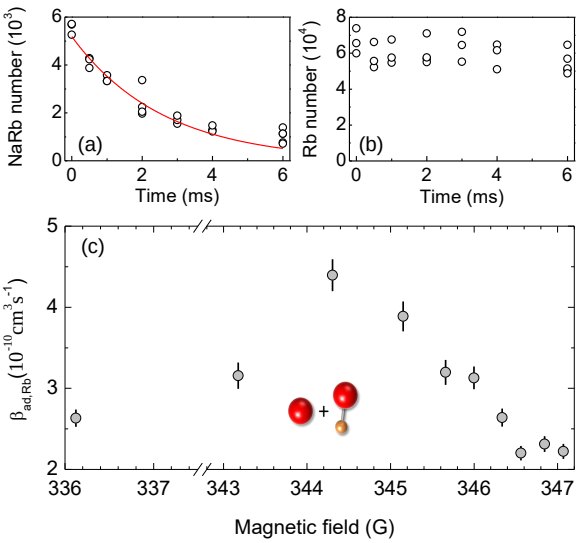

FIG. 2. Magnetic field dependence of the Rb-NaRb collisions. (a) and (b) show the time evolution of the number of NaRb dimers and Rb atoms, respectively, at 344.31 G. The solid line in (a) shows the exponential fit of the data to Eq. (3). (c) shows the loss rate coefficient $\beta_{\mathrm{ad,Rb}}$ as a function of the magnetic field strength B. The error bars represent the uncertainties of the fits (see the solid line in (a)).

shows that $\beta_{\mathrm{ad,Rb}}$ exhibits a maximum away from the interspecies Feshbach resonance.

Using Eq. (1), Fig. 3(a) replots the data from Fig. 2(c) as a function of a. If the loss maximum at $a \approx 160 a_0$ is an Efimov resonance, then its lineshape can be described approximately by [41]

$$\beta_{\mathrm{ad,Rb}} = C \frac{\sinh(2\eta_*)}{\sin^2[s_0 \ln(a/a^*_{\mathrm{ad,Rb}})] + \sinh^2(\eta_*)} \frac{\hbar a}{m_{\mathrm{Na}}}. \tag{4}$$

Here C is a constant, s_0 is equal to 0.87 for the mass ratio $\kappa = 3.78$, $a^*_{\mathrm{ad,Rb}}$ is the atom-dimer resonance position, and η_* is the linewidth of the resonance. Strictly speaking, Eq. (4) is derived for $T = 0$; thus, it may not fully reproduce the lineshape of the experimental finite temperature data. Moreover, the resonance position extracted from the fit should be interpreted as an estimate and not as the definite zero-temperature resonance position. The fit (solid line in Fig. 3(a)) yields $a^*_{\mathrm{ad,Rb}} = 171(3) a_0$ and $\eta_* = 0.32(1)$.

We have also studied Na atom and NaRb molecule collisions following a similar procedure. However, the removal of residual Rb atoms requires longer light pulses than the removal of residual Na atoms due to the smaller photon recoil and larger optical trap depth. This inevitably causes some heating and loss of FMs. As a result, the Na+NaRb mixture has a higher temperature and a lower signal to noise ratio than the Rb+NaRb mixture. Although we observed some hints of an atom-dimer loss peak, the poor signal to noise ratio prevented us from identifying it conclusively. We thus choose not to show

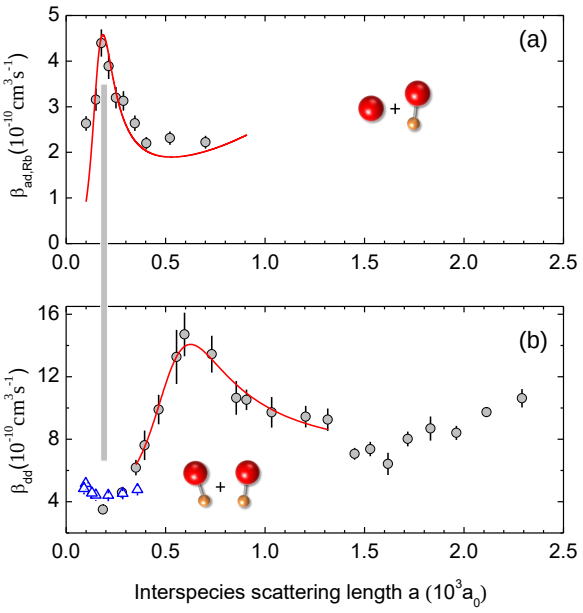

FIG. 3. (a) Atom-dimer loss rate coefficients $\beta_{\mathrm{ad,Rb}}$ vs a for Rb and NaRb collisions. The data are the same as those shown in Fig. 2(c). The solid curve is a fit to Eq. (4). (b) Dimer-dimer loss rate coefficient β_{dd} vs a for NaRb Feshbach molecule collisions. The filled circles, corresponding to $T = 730(30)$ nK, and the solid line are the same as those shown in Fig. 4(c). For comparison, the blue triangles at small a show results from data taken at a sample temperature of about 1 μK. All scattering lengths are calculated using the B-to-a conversion given in Eq. (1).

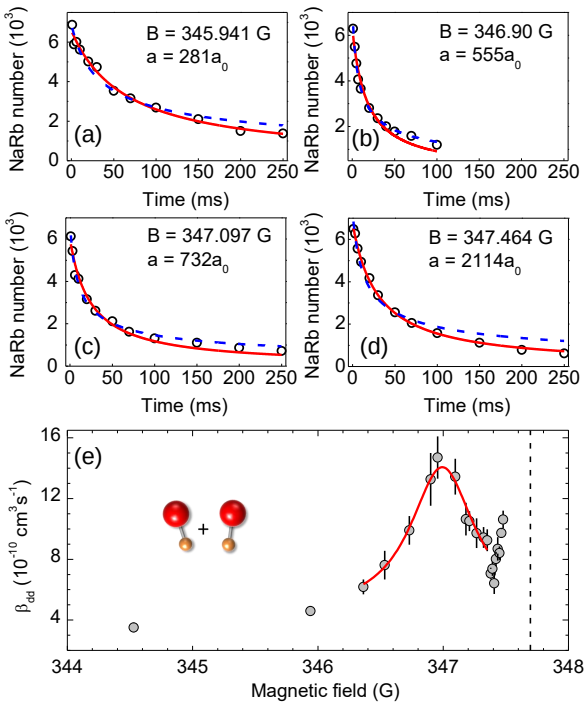

FIG. 4. Magnetic field dependent loss of pure NaRb FMs. (a)-(d) show the time evolution of the number of NaRb molecules for four selected magnetic field strengths, with (a) and (d) taken relatively far away from the observed loss maximum and with (b) and (c) taken relatively close to the observed loss maximum. The red solid and blue dashed curves are obtained by fitting the data by the two-body loss model [see Eq. (5)] and by the three-body loss model [see Eq. (6)], respectively. The symbols in (e) show the two-body dimer-dimer loss coefficient β_{dd}, extracted by fitting the experimental data by Eq. (5), as a function of the magnetic field field strength B. The error bars represent the uncertainties of the fits. The resonance position is determined by fitting the data near the loss maximum to a Lorentzian lineshape (red solid curve). The vertical dashed line marks the position of the Feshbach resonance.

the data here and relegate further investigations to the future.

C. Dimer-dimer collisions

To prepare a pure dimer sample, the residual Na and Rb atoms are removed by applying a strong magnetic field gradient pulse at 335.62 G right after the magneto-association [32]. At this magnetic field strength, the FMs have a near zero magnetic dipole moment and are thus nearly intact. Our experimental procedure routinely yields a pure molecular sample with up to 10^4 NaRb FMs. To measure the loss rate, the time evolution of the molecule number is recorded after ramping B from 335.62 G to the desired field strength.

Figures 4(a)-4(d) show the time evolution of the NaRb molecule number for four different magnetic field strengths. The loss time scale of the molecular sample is of the order of several 100 ms, i.e., it is notably longer than the loss time scale of the atom-dimer sample discussed in the previous section. Over their lifetime, the FMs can undergo several in-trap sloshing periods. The mean trap oscillation frequency measured from the sloshing motion is $\bar{\omega} = 2\pi \times 76(1)$ Hz. It shows no detectable dependence on the magnetic field strength. The typical sample temperature T is measured to be 730(30) nK by adding time-of-flight expansion before dissociating the molecules for detection. The calculated typical initial peak density is 1×10^{11} cm^{-3}.

In principle, the observed losses can be caused by several possible inelastic processes. Two colliding NaRb dimers can form either a Na_2Rb or a $NaRb_2$ trimer, with the fourth atom carrying away the released binding energy. Alternatively, one of the dimers can relax into a more deeply bound state, with the other dimer being dissociated. Both processes contribute, in principle, to two-body dimer loss [22]. Unfortunately, our measurements cannot distinguish whether one of these processes is dominant or whether both contribute appreciably. Near the magnetic field strengths at which the loss of dimers is maximal, the magnitude of the dimer-dimer scattering length a_{dd} is expected to be large. In this regime, the

loss of dimers may be triggered by collisions involving three dimers. We refer to this as three-body dimer loss. Without *a priori* assumption, it is not clear which, if any, of these processes dominates the loss of dimers from the molecular sample.

To determine the dimer loss processes, we model the measurements with both two-body and three-body loss equations. The red solid curves in Figs. 4(a)-4(d) show fits to the two-body rate equation

$$\frac{dN}{dt} = -\beta_{\rm dd} \langle n \rangle N = -\beta_{\rm dd} \frac{1}{\sqrt{8}} \left(\frac{M\bar{\omega}^2}{2\pi k_B T} \right)^{3/2} N^2, \quad (5)$$

where $\beta_{\rm dd}$ is the two-body dimer-dimer loss rate coefficient and $M = m_{\rm Rb} + m_{\rm Na}$ is the molecular mass. Circles in Fig. 4(e) show the extracted $\beta_{\rm dd}$ as a function of the magnetic field strength B. The data show a loss maximum at about 347 G, corresponding to $600a_0$. The blue dashed curves in Figs. 4(a)-4(d) show fits to the three-body rate equation

$$\frac{dN}{dt} = -\gamma_{\rm dd} \langle n^2 \rangle N = -\gamma_{\rm dd} \frac{1}{3\sqrt{3}} \left(\frac{M\bar{\omega}^2}{2\pi k_B T} \right)^{3} N^3, \quad (6)$$

where $\gamma_{\rm dd}$ denotes the three-body loss rate coefficient.

The quality of the fits reveals that the dominant loss mechanism changes with the magnetic field strength. The measurements shown in Figs. 4(a) and 4(d), which are taken at B field values where $\beta_{\rm dd}$ is small, are well described by the two-body model. The measurements shown in Fig. 4(b), which are taken at a B field value very close to that where $\beta_{\rm dd}$ is maximal, in contrast, are better described by the three-body model. Figure 4(c), which is taken at $B = 347.097$ G [just to the right of where $\beta_{\rm dd}$ takes its maximum; see Fig. 4(e)], shows an intermediate case where neither the two-body model nor the three-body model provide a fully satisfactory description of the data. The observation that three-body processes become more important as the magnetic field strength increases from $B = 345.941$ G to $B = 346.90$G and then become less important again as the magnetic field strength increases further is taken as evidence that the dimer-dimer scattering length is strongly dependent on the magnetic field strength. This suggests the existence of a dimer-dimer Feshbach resonance. As further supported by our theoretical modeling in Sec. III B, the magnetic field strength at which the loss peak is centered corresponds to the critical scattering length $a^*_{\rm dd}$ at which the Na_2Rb_2 state intercepts the NaRb+NaRb curve in Fig. 1.

The above analysis comes with a caveat. Even if the measurements are well described by a model that accounts for only one loss process, contributions from the other process may also play a role. We tried to extract both loss rate coefficients simultaneously by fitting to a model that includes both two- and three-body losses. However, the error bars of the loss rate coefficients obtained in this manner tend to be too large to extract reliable information. For data taken away from the loss maximum, the resulting $\gamma_{\rm dd}$ is, in some cases, negative. This indicates that three-body losses are significant only near the loss resonance. Since we were not able to determine a clear transition point from two-body dominated to three-body dominated loss, our analysis of the molecule loss from a pure dimer sample is based on the fits to the two-body model shown in Fig. 4(e). Because of this, the $\beta_{\rm dd}$ values in Fig. 4(e), especially near the loss maximum, should be viewed as effective two-body loss rate coefficients that may be "contaminated" to varying degrees by three-body contributions.

Equations (5) and (6) assume a Gaussian distribution for a thermal sample in a harmonic trap. However, even at the loss minimum near 344.5 G, where three-body contributions should be negligible, $\beta_{\rm dd}$ is quite large, $\beta_{\rm dd} \approx 3.5 \times 10^{-10}$ cm^{3}s^{-1}. Such a fast loss rate likely leaves the sample insufficient time to equilibrate, introducing a potentially large systematic error into $\beta_{\rm dd}$. We do not, unfortunately, have a good way to estimate this error. In addition, our analysis ignored the heating that typically accompanies inelastic collisions. Due to the anti-evaporation effect, the molecules removed have, on average, a lower energy than those that remain in the sample [42]. Our estimates suggest that this heating effect increases $\beta_{\rm dd}$ by less than 10%.

To extract the resonance position from the data shown in Fig. 4(e), we fit the data near the loss maximum to a Lorentzian function. This yields a resonance position of 346.99(1) G or, using Eq. (1), $a^*_{\rm dd} = 625(15)a_0$. The resulting fit [solid line in Fig. 4(e)] describes the data quite well. We stress that this functional form is empirical and not motivated by theoretical arguments. Figure 3(b) replots, using the B-to-a conversion given in Eq. (1), the data from Fig. 4(e) as a function of the interspecies scattering length a.

III. THEORY

A. Three-body system with zero-range two-body interactions

In our first set of calculations, the $NaRb_2$ system is treated in the adiabatic hyperspherical approximation [43–45] with two-body zero-range inter- and intraspecies interactions. Figure 5 shows the two lowest effective adiabatic potential curves as a function of the hyperradius R for a fixed Rb-Rb scattering length and various interspecies scattering lengths a, namely $a/a_{\rm RbRb} = 100, 4, 2$ and 1.7. The hyperradius R is defined as $R^2 = d^{-2}(r_{13})^2 + d^2(r_{13,2})^2$, where r_{13} denotes the distance between the Na atom (atom 3) and one of the Rb atoms (atom 1) and $r_{13,2}$ denotes the distance between the center of mass of the 13 subunit and the second Rb atom (atom 2). The mass scale d is defined as $d^2 = \mu_{13,2}/\mu_R$, where $\mu_{13,2} = (m_{\rm Rb} + m_{\rm Na})m_{\rm Rb}/(2m_{\rm Rb} + m_{\rm Na})$ is the reduced mass associated with the Jacobi distance $r_{13,2}$ and μ_R the hyperradial mass [$\mu_R^2 = m_{\rm Rb}^2 m_{\rm Na}/(2m_{\rm Rb} + m_{\rm Na})$].

Figure 5 scales the hyperradius by $a_{\rm RbRb}$ and the energy by $E_{\rm scale} = \hbar^2/[m_{\rm Na}(a_{\rm RbRb})^2]$.

The lowest adiabatic potential curve (dashed lines) approaches the Rb_2 dimer energy at large R for all a and negative infinity as R goes to zero, indicating that the Hamiltonian needs to be supplemented by a three-body parameter to avoid the Thomas collapse. The three-body states that "live" in these potential curves are referred to as belonging to the first or lower Efimov branch. The second lowest potential curve (solid lines), in contrast, approaches the NaRb dimer energy at large R for all a. This NaRb dimer threshold lies above the Rb_2 threshold for the a considered; it crosses the Rb_2 threshold at $a = 1.546 a_{\rm RbRb}$, i.e., at an interspecies scattering length that is somewhat smaller than those considered in Fig. 5. The solid lines exhibit a minimum around $R \approx 3-4 a_{\rm RbRb}$ and approach positive infinity as R goes to zero. The three-body states that live in these potential curves are referred to as belonging to the second or upper Efimov branch. The repulsive small-R behavior implies that one can, within the adiabatic hyperspherical approximation, calculate the $NaRb_2$ energies for the zero-range interaction model based solely on the two-body scattering lengths.

Since the experiments discussed in Sec. II B are conducted using a mixture of Rb atoms and NaRb dimers, we calculate the three-body energies in the second lowest adiabatic potential curves and search for the scattering length at which the $NaRb_2$ trimer energy is equal to the NaRb dimer energy, i.e., we search for the scattering length ratio $a/a_{\rm RbRb}$ at which the adiabatic potential curves shown by solid lines in Fig. 5 cease to support a three-body bound state. We find that this occurs at $a = a^*_{\rm ad,Rb} \approx 1.72 a_{\rm RbRb}$ or, plugging in the Rb-Rb scattering length for the experimentally relevant resonance, at $a^*_{\rm ad,Rb} \approx 173 a_0$. This parameter-free zero-range prediction agrees well with the experimentally measured value of $a^*_{\rm ad,Rb} \approx 171 a_0$.

It should be kept in mind that the adiabatic hyperspherical approximation is, as the name indicates, an approximation. Inclusion of the adiabatic correction changes the critical scattering length prediction by about 5%, i.e., we find $a^*_{\rm ad,Rb} \approx 1.81 a_{\rm RbRb}$ (we note that the percentage corrections are larger for the critical scattering lengths associated with excited states). While the relatively small change upon inclusion of the adiabatic correction may be interpreted as suggesting that the adiabatic hyperspherical approximation makes quantitative predictions, we cautiously note that these values cannot, since we are dealing with excited states, be interpreted as lower and upper bounds [46]. In principle, the entire set of adiabatic potential curves and associated channel couplings should be taken into account. Such a calculation is, however, not pursued here. One of the reasons is that the zero-range approximation itself needs to be extended to account for finite-range effects. Our premise is that the adiabatic hyperspherical framework provides physical insights as well as estimates for the critical scattering lengths that can be used to qualitatively, and possibly semi-quantitatively, explain aspects of the experimental results.

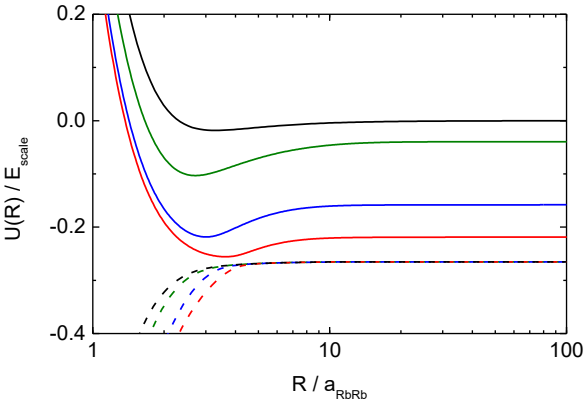

FIG. 5. Effective adiabatic hyperspherical potential curves $U(R)$ for the $NaRb_2$ system with zero-range interactions. The scattering length ratios considered are $a/a_{\rm RbRb} = 100$ (black), 4 (green), 2 (blue), and 1.7 (red), from top to bottom for both the solid and the dashed lines. The potential curves shown by dashed and solid lines correspond to the lower Efimov branch and the upper Efimov branch, respectively. The dashed lines approach the Rb_2 dimer energy of $-\kappa^{-1} E_{\rm scale} = -0.2645 E_{\rm scale}$ at large R. The solid lines approach the NaRb dimer energy of $-(1+\kappa^{-1})(a_{\rm RbRb}/a)^2 E_{\rm scale}/2 = -0.6323(a_{\rm RbRb}/a)^2 E_{\rm scale}$ at large R.

In addition to the critical scattering length $a^*_{\rm ad,Rb}$ associated with the lowest $NaRb_2$ trimer state of the second Efimov branch, we used the adiabatic potential curves to calculate other critical scattering lengths. The next three higher-lying trimers hit the atom-dimer threshold at $a/a_{\rm RbRb} \approx 29$, $a/a_{\rm RbRb} \approx 1250$, and $a/a_{\rm RbRb} \approx 47000$, yielding for the scattering length ratios approximately 1/17 for the lowest two states, 1/43 for the second- and third-lowest states, and 1/38 for the next pair of states. These values suggest that the finite value of the Rb-Rb scattering length has a profound effect on the scattering length ratios on the positive interspecies scattering lengths side. Qualitatively, this can be understood by realizing that the lowest trimer state at the atom-dimer threshold has three "active" interactions with approximately equal scattering length (the scaling factor for three resonant interactions is $\lambda = 16.12$) while the higher-lying states at the atom-dimer threshold resemble more and more the situation where only two interactions are "active" (recall, the scaling factor for two resonant interactions is $\lambda_{\rm NaRbRb} = 37$).

For completeness, we also report the scattering lengths for the two lowest states for which the trimers hit the three-atom threshold on the negative interspecies scattering length side. The values are $a^-_{\rm Rb} \approx -118 a_{\rm RbRb}$ and $-4085 a_{\rm RbRb}$, yielding a ratio of 1/34.6 and suggesting that the experimental observation of the first three-atom loss feature may already require rather good magnetic field control. In addition, there may exist three-atom loss

features that are associated with three-body states that live in the lower Efimov branch; these are not considered here.

We also treated the Na_2Rb system in the adiabatic hyperspherical approximation. For the upper Efimov branch (this is the branch for which the corresponding adiabatic hyperspherical potential curves approach the NaRb dimer energy at large R), the lowest trimer hits the atom-dimer threshold at $a^*_{\rm ad,Na} \approx 2.8 a_{\rm RbRb}$ and the three-atom threshold at $a^-_{\rm Na} \approx -40300 a_{\rm RbRb}$. Combining the $NaRb_2$ and Na_2Rb results, the adiabatic hyperspherical framework predicts $a^*_{\rm ad,Na}/a^*_{\rm ad,Rb} \approx 2.8/1.72 \approx 1.63$. We note that the critical scattering length $a^*_{\rm ad,Na}$ depends quite sensitively on corrections beyond the adiabatic hyperspherical approximation, suggesting that it is quite possible that the ratio $a^*_{\rm ad,Na}/a^*_{\rm ad,Rb}$ is larger than 1.63.

The description of the three-body system could be made more quantitative by constructing a Hamiltonian that employs finite-range two-body model interactions with the correct scattering lengths and van der Waals tails. While this is a worthwhile avenue to pursue, solving the corresponding four-body Schrödinger equation is a rather challenging task that is not pursued here. Instead, the next section develops a simple finite-range framework for which the four-body Schrödinger equation can be solved fairly straightforwardly.

B. Finite-range low-energy model

Section III A suggests that the experimentally observed atom-dimer loss feature is associated with the lowest $NaRb_2$ trimer in the second Efimov branch. To treat the Na_2Rb_2 and $NaRb_3$ tetramers, we employ a finite-range model that excludes both Rb_2 dimers and Na_2 dimers. As a consequence, the model describes the $NaRb_2$ and Na_2Rb trimers that live in the upper Efimov branch but not those that live in the lower Efimov branch.

The model assumes that each Rb-Na pair interacts through an attractive two-body Gaussian potential with fixed range r_0 and variable depth v_0; the depth v_0 is adjusted to dial in the desired value of the interspecies scattering length a. In addition, each Na-Rb-Rb triple interacts through a purely repulsive Gaussian three-body potential with range R_0 and height $V_{0,\rm Rb}$ [21] (note this three-body interaction potential is distinct from the effective adiabatic potentials discussed in Sec. III A). Similarly, each Na-Na-Rb triple interacts through a purely repulsive Gaussian three-body potential with the same range R_0 and height $V_{0,\rm Na}$. Throughout, the range R_0 is fixed. The height $V_{0,\rm Rb}$, which serves to set the energy scale of the $NaRb_2$ trimer, is also fixed and choosen such that the interspecies scattering length a at which the $NaRb_2$ trimer energy hits the atom-dimer threshold is a few times larger than r_0 and R_0; this separation of scales ensures that the results are, to a good approximation, independent of the details of the model potentials. The height $V_{0,\rm Na}$, in turn, is varied. For each fixed $V_{0,\rm Na}$, the Na_2Rb trimer and Na_2Rb_2 tetramer energies are calculated as a function of a and the critical scattering lengths $a^*_{\rm ad,Rb}$ and $a^*_{\rm dd}$ are determined. The strategy is then to choose the "best" $V_{0,\rm Na}$ such that the ratio $a^*_{\rm ad,Rb}/a^*_{\rm ad,Na}$ is roughly the same as that for the zero-range model. The critical scattering length $a^*_{\rm dd}$ obtained in this manner is a prediction of this low-energy model Hamiltonian. Note that the critical scattering length at which the $NaRb_2$ trimer and the $NaRb_3$ tetramer become unbound is independent of $V_{0,\rm Na}$.

The idea behind the finite-range low-energy interaction model is that the repulsive Rb-Rb scattering length is accounted for, in an effective manner, by a purely repulsive three-body potential that introduces a repulsive short-range repulsion in the adiabatic potential curve for the $NaRb_2$ system. Similarly, the repulsive Na-Na scattering length is accounted for, again in an effective manner, by a purely repulsive three-body potential that introduces a repulsive short-range repulsion in the adiabatic potential curve for the Na_2Rb system. Adjusting $V_{0,\rm Na}$ while keeping $V_{0,\rm Rb}$ fixed then allows one to "dial in" the desired relative strengths of these short-range repulsions. We refer to this model as a low-energy model since the deeper-lying Na_2 and Rb_2 thresholds are not accounted for at all, excluding, e.g., the possibility that the Na_2Rb_2 tetramer breaks up into Na_2 and Rb_2.

We solve the time-independent Schrödinger equation for the low-energy Hamiltonian by a basis set expansion approach, namely, we use explicitly correlated Gaussian basis functions with non-linear parameters that are optimized semi-stochastically [47, 48]. Figure 6 shows the three- and four-body energies—with the threshold energies subtracted—for our finite-range model. Pluses show the energy difference $E_{\rm NaRb_2} - E_{\rm NaRb}$ as a function of r_0/a while triangles show the energy difference $E_{\rm NaRb_2} - 2E_{\rm NaRb}$ as a function of r_0/a, where $E_{\rm NaRb_2}$ is the lowest $NaRb_2$ trimer energy of our model Hamiltonian. The points at which these energy differences vanish are the critical scattering length values. On the negative scattering length side, this is the critical scattering length $a^-_{\rm Rb}$ and on the positive scattering length side, these are the critical scattering lengths $a^*_{\rm ad,Rb}$ and $a^{\rm reaction}_{\rm dd,Rb}$, corresponding to the square in Fig. 1 (i.e., the scattering length at which the rearrangement reaction NaRb + NaRb $\rightarrow$ $NaRb_2$ + Rb is expected to be enhanced). The model predicts the scattering length ratio $a^{\rm reaction}_{\rm dd,Rb}/a^*_{\rm ad,Rb} \approx 8$ (in the zero-range model, this ratio is about 10 in the hyperspherical approximation and 7 if the adiabatic correction is included) and a ratio of about 20 for the atom-dimer resonance positions of the two lowest states (recall, the zero-range model, treated in the adiabatic approximation, yielded ≈ 17). These comparisons show that our finite-range model reproduces the $NaRb_2$ trimer properties on the positive scattering length side predicted by the zero-range model quite well.

Our potential model predicts the existence of exactly one $NaRb_3$ tetramer state. The energy of this state is

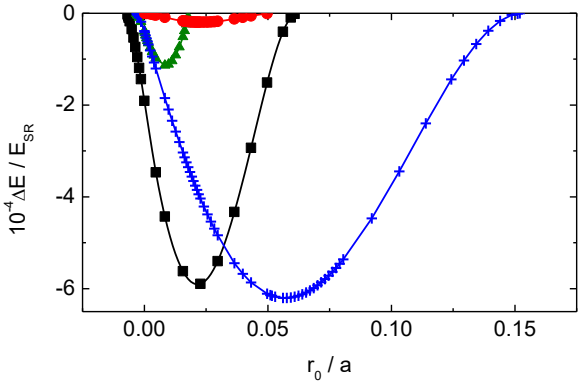

FIG. 6. Three- and four-body energies, relative to various thresholds, calculated using the low-energy finite-range Hamiltonian as a function of $1/a$. The pluses show the energy difference $\Delta E = E_{\mathrm{NaRb_2}} - E_{\mathrm{NaRb}}$; on the positive a side, the energy difference is zero at $a = a^*_{\mathrm{ad,Rb}}$. The circles show the energy difference $\Delta E = E_{\mathrm{Na_2Rb}} - E_{\mathrm{NaRb}}$; on the positive a side, the energy difference is zero at $a = a^*_{\mathrm{ad,Na}}$. The triangles show the energy difference $\Delta E = E_{\mathrm{NaRb_2}} - 2E_{\mathrm{NaRb}}$; on the positive a side, the energy difference is zero at the critical scattering length where the rearrangement reaction NaRb+NaRb $\rightarrow$ $\mathrm{NaRb_2}$+Na is enhanced. The squares show the energy difference $\Delta E = E_{\mathrm{Na_2Rb_2}} - 2E_{\mathrm{NaRb}}$; on the positive a side, the energy difference is zero at $a = a^*_{\mathrm{dd}}$. The low-energy Hamiltonian predicts $a^*_{\mathrm{dd}} > a^*_{\mathrm{ad,Rb}}$. The energy differences are scaled by $E_{\mathrm{SR}} = \hbar^2/(2\mu_{\mathrm{NaRb}} r_0^2)$, where μ_{NaRb} is the reduced mass of the NaRb dimer.

not shown in Fig. 6. Within our numerical accuracy, the $\mathrm{NaRb_3}$ tetramer becomes unbound at the same interspecies scattering length as the $\mathrm{NaRb_2}$ trimer.

Next we consider the $\mathrm{Na_2Rb}$ trimer and $\mathrm{Na_2Rb_2}$ tetramer, whose energies depend, within our model, on the three-body height $V_{0,\mathrm{Na}}$. The circles in Fig. 6 show the energy difference $E_{\mathrm{Na_2Rb}} - E_{\mathrm{NaRb}}$ for the height $V_{0,\mathrm{Na}}$ of the repulsive Na-Na-Rb potential chosen such that $a^*_{\mathrm{ad,Na}}$ is about three times larger than $a^*_{\mathrm{ad,Rb}}$. For this model Hamiltonian, the energy difference $E_{\mathrm{Na_2Rb_2}} - 2E_{\mathrm{NaRb}}$ (squares in Fig. 6) goes to zero at $a = a^*_{\mathrm{dd}} \approx 2.45 a^*_{\mathrm{ad,Rb}}$. If $V_{0,\mathrm{Na}}$ is chosen such that $a^*_{\mathrm{ad,Na}}$ is about two times larger than $a^*_{\mathrm{ad,Rb}}$, we find $a = a^*_{\mathrm{dd}} \approx 2.17 a^*_{\mathrm{ad,Rb}}$ (recall, the zero-range model in the adiabatic approximation predicts $a^*_{\mathrm{ad,Na}}/a^*_{\mathrm{ad,Rb}} = 1.63$; the actual value, however, is—as discussed in Sec. III A—expected to be somewhat larger). This shows that a^*_{dd} depends, if expressed in terms of $a^*_{\mathrm{ad,Rb}}$, less strongly on the value of $V_{0,\mathrm{Na}}$ than $a^*_{\mathrm{ad,Na}}$, suggesting that the $\mathrm{Na_2Rb_2}$ tetramer properties are primarily determined by the properties of the $\mathrm{NaRb_2}$ trimer. Our calculations suggest that a^*_{dd} is larger than $a^*_{\mathrm{ad,Rb}}$. We cannot determine unambiguously whether a^*_{dd} is greater or smaller than $a^*_{\mathrm{ad,Na}}$, primarily because the zero-range prediction for $a^*_{\mathrm{ad,Na}}$ depends sensitively on whether or not the adiabatic correction is included. Our potential model, using what we consider reasonable values for $V_{0,\mathrm{Na}}$, predicts the existence of exactly one $\mathrm{Na_2Rb_2}$ tetramer state.

IV. DISCUSSIONS

Table I summarizes the experimentally and theoretically obtained resonance positions. For the Rb-NaRb resonance, the parameter-free zero-range prediction of $a^*_{\mathrm{ad,Rb}} = 173 a_0$ agrees well with the experimentally measured value of $171 a_0$, despite the non-universal character of the FMs near such small a [32]. Moreover, the zero-range and finite-range models predict that the next Rb-NaRb resonance is located at $a^*_{\mathrm{ad,Rb,1}} \approx 3000 a_0$; this moderately large interspecies scattering length should be accessible with the improved magnetic field system that is currently being constructed in our laboratory.

Using an empirical fit to the dimer-dimer loss coefficient β_{dd}, which was extracted from the experimental data assuming a two-body loss model, we determined the dimer-dimer resonance position to be located at $a^*_{\mathrm{dd}} = 625 a_0$. This value is nearly 50% larger than the value of $420 a_0$ predicted by the finite-range model. The fact that both the experimental data and the theoretical model exhibit a dimer-dimer resonance, albeit at somewhat different scattering lengths, is very encouraging. The fact that the agreement is, at present, at the qualitative and not at the quantitative level is not surprising given that the experiment operates at finite temperature, that the analysis of the experimental data is based on a model that does not account for three-body loss processes, and that the finite-range model makes a number of simplifying assumptions regarding the four-body dynamics.

The dimer-dimer loss rate coefficient β_{dd} [see Fig. 3(b)] decreases from its maximum at $a = 625 a_0$ to a local minimum at around $a = 1600 a_0$ and then increases again approximately linearly with increasing a. Beyond $a = 2350 a_0$, no experimental information is presently available for the Na-Rb mixture. The experimental data provide no evidence for the existence of a loss maximum due to the rearrangement reaction NaRb+NaRb $\rightarrow$ $\mathrm{NaRb_2}$+Rb, which is predicted to occur at $a \approx 1400 a_0$ according to the finite-range model and at $a \approx 1750 a_0$ according to the zero-range model. One explanation could be that the rearrangment reaction occurs at larger a than those covered in the experiment. An alternative explanation could be that the associated loss peak is not very pronounced, i.e., that a finer magnetic field scan with improved analysis of the experimental data is needed. A third explanation could be that the model Hamiltonian underlying the theoretical calculations neglect important microscopic details.

We note that the dimer-dimer loss feature that is located at around $625 a_0$ has a shape similar to that calculated for homonuclear bosonic $\mathrm{Cs_2}$ FMs [26]; the resonance observed in our work corresponds to the first $\mathrm{Cs_2} + \mathrm{Cs_2} \rightarrow \mathrm{Cs_4}$ resonance [$a^*_{\mathrm{dd},1}$ in Fig. 2(b) of Ref. [26]]. In the homonuclear case, a second resonance is caused by a more weakly-bound second tetramer near the threshold of the $\mathrm{Cs_2} + \mathrm{Cs_2} \rightarrow \mathrm{Cs_3} + \mathrm{Cs}$ rearrangement reaction. As discussed in Sec. III B, there exists only one $\mathrm{Na_2Rb_2}$

TABLE I. Summary of the calculated and observed few-body resonances in the Na-Rb system. The results in the column labeled "zero range" are obtained using the zero-range two-body interaction model introduced in Sec. III A while those in the column labeled "finite range" are obtained using the finite-range low-energy model introduced in Sec. III B. The interspecies scattering length at which the second Rb-NaRb resonance is predicted to exist is denoted by $a^*_{\mathrm{ad,Rb,1}}$. In the column labeled "experiment", the unexplored regions are left blank while the regions covered in the current investigation, but without confirmed resonances, are marked by crosses.

resonances	zero range	finite range	experiment
$a^*_{\mathrm{ad,Rb}}$	$173a_0$		$171(3)a_0$
$a^*_{\mathrm{ad,Rb,1}}$	$2941a_0$	$3460a_0$	
$a^*_{\mathrm{ad,Na}}$	$281a_0$		$\times$
a^*_{dd}		$\sim 420a_0$	$625(15)a_0$
$a^{\mathrm{reaction}}_{\mathrm{dd,Rb}}$	$1730a_0$	$1384a_0$	$\times$
a^-_{Rb}		$\sim -11850a_0$	
a^-_{Na}		$\sim -4.05\times10^6a_0$	

tetramer state in our system but two rearrangement reactions, i.e., NaRb+NaRb→ $NaRb_2$+Na and NaRb+NaRb → Na_2Rb+Rb, might be possible.

Due to these NaRb+NaRb rearrangement reactions, strong molecule losses for a range of a near the Feshbach resonance should be expected. This is expected to severely limit the lifetime of the NaRb FM sample. However, these rearrangement reactions may also have some useful applications, e.g., for the creation of $NaRb_2$ and Na_2Rb trimers starting from NaRb FMs [26]. Since the energy released by the two rearrangement reactions is negligible, both trimers should remain, assuming realistic trap parameters, trapped for further investigations, although the lifetime of the trimers may be short. With improved magnetic field stability, which should become available in the near future, the rearrangement reactions can be confirmed by observing the appearance of Rb or Na atoms for pure NaRb samples [26].

The theoretical calculations from Ref. [26] for a pure Cs system suggest that the dimer-dimer loss rate coefficient shows a minimum at the Cs-Cs scattering length at which the atom-dimer resonance happens. Corresponding experimental results for the dimer-dimer loss minimum [25] and the atom-dimer resonance [40] were reported in two consecutive publications. Comparing the scattering length values at which these resonances are located ($a \approx 500a_0$ and $a \approx 367a_0$, respectively), one concludes that the features lie close to each other. Intriguingly, an analogous correspondence between the dimer-dimer loss minimum and the atom-dimer resonance is observed in our Na-Rb system (see the thick grey vertical line in Fig. 3). To confirm this feature, we take another set of dimer-dimer collision data near $a = a^*_{\mathrm{ad,Rb}}$ with finer step size. The resulting data, taken at a temperature of about $\sim$ 1 μK, are shown by triangles in Fig. 3(b). Although the sample temperature for the new data is higher than for the first data set, the minimum near $a = a^*_{\mathrm{ad,Rb}}$ is reproduced unambiguously. The fact that the dimer-dimer loss rate coefficient shows a minimum at or near the scattering length at which the atom-dimer resonance happens in both homonuclear and heteronuclear systems may indicate some universal relation between these three-and four-body processes. Currently, this is not fully understood and more theoretical and experimental work is needed.

V. OUTLOOK

The experimental confirmation of long-predicted three-body Efimov resonances in dilute ultracold gases is a great triumph for the field of few-body physics. While the Efimov scenario—and extensions thereof to more particles—is most frequently discussed for identical bosons, the Efimov scenario for bosonic and fermionic mixtures has been studied theoretically from the very beginning. Moreover, recent years have seen markedly increased experimental efforts in preparing dual-species systems, resulting in the experimental observation of three-body Efimov resonances in mixed-species systems. These initial studies indicated that the few-body physics in mixtures is qualitatively different from that in homonuclear systems and that additional studies of bosonic and fermionic mixtures in the three- and higher-body sectors are needed to develop a solid understanding of how Efimov physics manifests itself in cold atom mixtures. The present work responded to this need and experimentally and theoretically studied several previously unexplored few-body processes with an ultracold Bose-Bose mixture consisting of sodium and rubidium atoms and weakly-bound NaRb Feshbach dimers. Our results for this Bose-Bose mixture not only testify again the wealthiness of few-body physics in heteronuclear mixtures but they also have several important implications and motivate possible applications.

Just as the atom-atom Feshbach resonance allows one to control the effective atom-atom interaction strength, the dimer-dimer resonance can be used to control the effective interaction strength between two weakly-bound NaRb FMs. Going from B values that are smaller than the magnetic field strength corresponding to a^*_{dd} to B values that are larger than the magnetic field strength corresponding to a^*_{dd}, the dimer-dimer scattering length a_{dd} can be tuned from positive to negative. In this sense, the current experiment already created FMs with attractive interactions even though the atom-atom scattering length remains positive, corresponding to an effective repulsive atom-atom interaction [26]. This counter-intuitive behavior can be quantified experimentally and understood in a similar manner as for the atom-dimer system [49]. An interesting question is whether it is possible to observe three-dimer Efimov resonances near a^*_{dd}, in analogy to three-atom Efimov resonances, i.e., Efimov resonances on the negative dimer-dimer scattering length side that originate from the energetic degeneracy of the

hexamer state and the three-dimer system.

The low-energy sector of the homonuclear four-boson system with, in absolute value, large atom-atom scattering length has been shown to behave universally. This implies that the dimer-dimer resonances, the scattering lengths at which rearrangement reactions are favored, and the atom-dimer resonances are related via simple universal relations [3, 26, 50]. Whether analogous universal relations hold for the heteronuclear case and if they do, how these relations scale with the mass ratio, are open questions. In answering these questions, it is expected that the background intraspecies scattering lengths and finite-temperature effects need to be considered carefully [20]. The work presented in this paper lays the groundwork for future explorations of heteronuclear few-body systems, which can be viewed as building blocks of larger systems.

Importantly, our observations have valuable implications for a more efficient production of bosonic FMs from ultracold atom samples. When the magnetic field is ramped across the interspecies Feshbach resonance during the magneto-association, unavoidably there exist various inelastic few-body processes that can lead to detremental molecule loss. Radio frequency association [51], for instance in our system near the local dimer-dimer loss minimum at $1600a_0$, should be able to partially mitigate the loss problem. If the association step can be made sufficiently efficient, obtaining a larger molecular sample should be feasible.

ACKNOWLEDGMENTS

We thank P. S. Julienne, C. H. Greene and J. P. D'Incao for valuable discussions, and Bing Zhu and Bo Lu for laboratory assistance. This work was supported by the French ANR/Hong Kong RGC COPOMOL project (grant no. A-CUHK403/13), the RGC General Research Fund (grant no. CUHK14301815), and the US National Science Foundation (grant no. PHY-1509892).

[1] V. Efimov, Phys. Lett. B **33**, 563 (1970).
[2] T. Kraemer, M. Mark, P. Waldburger, J. Danzl, C. Chin, B. Engeser, A. Lange, K. Pilch, A. Jaakkola, H.-C. Nägerl, and R. Grimm, Nature **440**, 315 (2006).
[3] E. Braaten and H.-W. Hammer, Phys. Rep. **428**, 259 (2006).
[4] V. Efimov, Sov. J. Nucl. Phys. **12**, 589 (1971).
[5] V. Efimov, Nucl. Phys. A **210**, 157 (1973).
[6] J. P. D'Incao and B. D. Esry, Phys. Rev. A **73**, 030703 (2006).
[7] C. Chin, R. Grimm, P. Julienne, and E. Tiesinga, Rev. Mod. Phys. **82**, 1225 (2010).
[8] S. E. Pollack, D. Dries, and R. G. Hulet, Science **326**, 1683 (2009).
[9] M. Zaccanti, B. Deissler, C. D'Errico, M. Fattori, M. Jona-Lasinio, S. Müller, G. Roati, M. Inguscio, and G. Modugno, Nature Phys. **5**, 586 (2009).
[10] N. Gross, Z. Shotan, S. Kokkelmans, and L. Khaykovich, Phys. Rev. Lett. **103**, 163202 (2009).
[11] R. J. Wild, P. Makotyn, J. M. Pino, E. A. Cornell, and D. S. Jin, Phys. Rev. Lett. **108**, 145305 (2012).
[12] S. Roy, M. Landini, A. Trenkwalder, G. Semeghini, G. Spagnolli, A. Simoni, M. Fattori, M. Inguscio, and G. Modugno, Phys. Rev. Lett. **111**, 053202 (2013).
[13] G. Barontini, C. Weber, F. Rabatti, J. Catani, G. Thalhammer, M. Inguscio, and F. Minardi, Phys. Rev. Lett. **103**, 043201 (2009).
[14] R. S. Bloom, M.-G. Hu, T. D. Cumby, and D. S. Jin, Phys. Rev. Lett. **111**, 105301 (2013).
[15] S.-K. Tung, K. Jiménez-García, J. Johansen, C. V. Parker, and C. Chin, Phys. Rev. Lett. **113**, 240402 (2014).
[16] R. Pires, J. Ulmanis, S. Häfner, M. Repp, A. Arias, E. D. Kuhnle, and M. Weidemüller, Phys. Rev. Lett. **112**, 250404 (2014).
[17] R. A. W. Maier, M. Eisele, E. Tiemann, and C. Zimmermann, Phys. Rev. Lett. **115**, 043201 (2015).
[18] L. J. Wacker, N. B. Jørgensen, D. Birkmose, N. Winter, M. Mikkelsen, J. Sherson, N. Zinner, and J. J. Arlt, Phys. Rev. Lett. **117**, 163201 (2016).
[19] J. Ulmanis, S. Häfner, R. Pires, F. Werner, D. S. Petrov, E. D. Kuhnle, and M. Weidemüller, Phys. Rev. A **93**, 022707 (2016).
[20] J. Ulmanis, S. Häfner, R. Pires, E. D. Kuhnle, Y. Wang, C. H. Greene, and M. Weidemüller, Phys. Rev. Lett. **117**, 153201 (2016).
[21] D. Blume and Y. Yan, Phys. Rev. Lett. **113**, 213201 (2014).
[22] B. Marcelis, S. J. J. M. F. Kokkelmans, G. V. Shlyapnikov, and D. S. Petrov, Phys. Rev. A **77**, 032707 (2008).
[23] Y. Wang, W. B. Laing, J. von Stecher, and B. D. Esry, Phys. Rev. Lett. **108**, 073201 (2012).
[24] C. Chin, T. Kraemer, M. Mark, J. Herbig, P. Waldburger, H.-C. Nägerl, and R. Grimm, Phys. Rev. Lett. **94**, 123201 (2005).
[25] F. Ferlaino, S. Knoop, M. Mark, M. Berninger, H. Schöbel, H.-C. Nägerl, and R. Grimm, Phys. Rev. Lett. **101**, 023201 (2008).
[26] J. P. D'Incao, J. von Stecher, and C. H. Greene, Phys. Rev. Lett. **103**, 033004 (2009).
[27] H.-W. Hammer and L. Platter, Eur. Phys. J. A **32**, 113 (2007).
[28] J. von Stecher, J. P. D'Incao, and C. H. Greene, Nature Phys. **5**, 417 (2009).
[29] F. Ferlaino, S. Knoop, M. Berninger, W. Harm, J. P. D'Incao, H.-C. Nägerl, and R. Grimm, Phys. Rev. Lett. **102**, 140401 (2009).
[30] F. Wang, D. Xiong, X. Li, D. Wang, and E. Tiemann, Phys. Rev. A(R) **87**, 050702 (2013).
[31] F. Wang, X. Li, D. Xiong, and D. Wang, J. Phys. B **49**, 015302 (2015).
[32] F. Wang, X. He, X. Li, B. Zhu, J. Chen, and D. Wang, New J. Phys. **17**, 035003 (2015).
[33] J. Wang, J. P. D'Incao, B. D. Esry, and C. H. Greene, Phys. Rev. Lett. **108**, 263001 (2012).

[34] P. Naidon, S. Endo, and M. Ueda, Phys. Rev. Lett. **112**, 105301 (2014).
[35] P. Naidon, S. Endo, and M. Ueda, Phys. Rev. A **90**, 022106 (2014).
[36] Y. Wang, J. Wang, J. P. D'Incao, and C. H. Greene, Phys. Rev. Lett. **109**, 243201 (2012).
[37] Y. Wang, J. Wang, J. P. D'Incao, and C. H. Greene, Phys. Rev. Lett. **115**, 069901 (2015).
[38] E. G. M. van Kempen, S. J. J. M. F. Kokkelmans, D. J. Heinzen, and B. J. Verhaar, Phys. Rev. Lett. **88**, 093201 (2002).
[39] S. Knoop, T. Schuster, R. Scelle, A. Trautmann, J. Appmeier, M. Oberthaler, E. Tiesinga, and E. Tiemann, Physical Review A **83**, 042704 (2011).
[40] S. Knoop, F. Ferlaino, M. Mark, M. Berninger, H. Schöbel, H.-C. Nägerl, and R. Grimm, Nature Phys. **5**, 227 (2009).
[41] K. Helfrich, H.-W. Hammer, and D. S. Petrov, Phys. Rev. A **81**, 042715 (2010).
[42] T. Weber, J. Herbig, M. Mark, H.-C. Nägerl, and R. Grimm, Phys. Rev. Lett. **91**, 123201 (2003).
[43] J. Macek, J. Phys. B **1**, 831 (1968).
[44] H. Klar and M. Klar, Phys. Rev. A **17**, 1007 (1978).
[45] A. F. Starace and G. L. Webster, Phys. Rev. A **19**, 1629 (1979).
[46] H. T. Coelho and J. E. Hornos, Phys. Rev. A **43**, 6379 (1991).
[47] Y. Suzuki and K. Varga, *Stochastic Variational Approach to Quantum-Mechanical Few-Body Problems*, 1st ed. (Springer-Verlag Berlin Heidelberg, 1998).
[48] J. Mitroy, S. Bubin, W. Horiuchi, Y. Suzuki, L. Adamowicz, W. Cencek, K. Szalewicz, J. Komasa, D. Blume, and K. Varga, Rev. Mod. Phys. **85**, 693 (2013).
[49] M. Jag, M. Zaccanti, M. Cetina, R. S. Lous, F. Schreck, R. Grimm, D. S. Petrov, and J. Levinsen, Phys. Rev. Lett. **112**, 075302 (2014).
[50] A. Deltuva, Phys. Rev. A **84**, 022703 (2011).
[51] S. T. Thompson, E. Hodby, and C. E. Wieman, Phys. Rev. Lett. **95**, 190404 (2005).